Flow in an Impeller-Stirred Tank Using an Immersed-Boundary Method

R. Verzicco
Dipartimento di Ingegneria Meccanica e Gestionale (DIMeG) and Centro di Eccellenza in Meccanica Computazionale (CEMeC), Politecnico di Bari, 70125, Bari, Italy

M. Fatica and G. Iaccarino
Center for Turbulence Research (CTR), Stanford University, Stanford, CA 94305

P. Orlandi
Dipartimento di Meccanica e Aeronautica (DMA), Università di Roma "La Sapienza," 00184, Rome, Italy

DOI 10.1002/aic.10117
Published online in Wiley InterScience (www.interscience.wiley.com).

The moderate Reynolds number flow developing in a cylindrical unbaffled stirred tank is studied using direct numerical simulation (DNS) and the results are compared with available experimental data and Reynolds Averaged Navier–Stokes (RANS) solutions. The geometry of the impeller is handled using an immersed-boundary procedure implemented in a solver written for cylindrical coordinates. This allows efficient simulation of the flow at a reasonable computational cost and accurate prediction of the mean and rms velocity fields. For this configuration, RANS performs poorly because of the low Reynolds and strongly unsteady and inhomogeneous nature of the flow: many different flow structures are produced, ranging from small-scale vortices generated at the blade tips to large-scale meridional recirculation. It is shown, in addition, that inaccurate results are produced by the wrong (computational) assumption that an impeller with n *blades produces instantaneous fields with an* n*-fold symmetry. Because simple stirred-tank configurations (like the present one) have been recently used to assess the performance of several RANS closures, the main message of this study is that simple geometrical configurations and low Reynolds numbers are not benign parameters for such a task.* © 2004 American Institute of Chemical Engineers *AIChE J,* 50: 1109–1118, 2004
Keywords: direct simulation, mixing device, transitional unsteady flow, turbulence modeling

Introduction

Stirred tanks are encountered in a wide variety of industrial processes from chemical reactors to biotechnologies; therefore, the understanding and prediction of the fluid dynamics of such devices is of key importance for future developments. Experimental investigations are generally limited to small-scale mixers that facilitate controlled conditions and accurate measurements. Computer simulation techniques, on the other hand, provide the opportunity to access the performance of real-world mixers at low cost. The difficulties associated with the numerical simulation of the turbulent flow in a stirred tank are: (1) relative motion of the impeller and the tank, (2) complex geometry of the

Correspondence concerning this article should be addressed to R. Verzicco at verzicco@poliba.it.

impeller, (3) turbulence modeling, and (4) large disparity of scales (in time and space) present.

Early studies avoided the simulation of the flow close to the impeller and adopted an approximate boundary condition based on experimental data (Xu and McGrath, 1996); the accuracy obtained is clearly a function of the available measurements. A more appropriate use of a direct boundary conditions (with the geometry of the impeller taken into account) was adopted in Harvey III and Rogers (1995, 1996), where steady and unsteady Navier–Stokes equations were solved on a body-fitted multiblock mesh. The results showed that a reasonable level of accuracy could be achieved for the radial and axial components of the velocity; nevertheless very fine grids and time-accurate simulations were required to capture correctly the tangential velocity, which was otherwise strongly overpredicted.

Turbulent simulations were carried out for a similar impeller configuration in Wechsler et al. (1999); unsteady Reynolds Averaged Navier–Stokes (RANS) equations closed by the standard κ–ε model with wall functions (Launder and Sharma, 1974) were used. Large-scale flow field structures were accurately reproduced, but only a fair agreement for the velocity and turbulent kinetic energy profile was obtained. This poses questions on the ability of the simple turbulence model used to account for the extremely complex turbulent mixing occurring in the tank. A comprehensive study on the effect of turbulence modeling was carried out by Jones et al. (2001) in an unbaffled stirred tank. Several closures were used, ranging from the standard κ–ε model with wall functions to low-Re κ–ε models; in spite of a large scatter between the predictions obtained with different models, none was able to correctly reproduce the velocity field in the close vicinity of the impeller. In addition, a large overprediction of the radial velocity is obtained independently from the model used. For the case studied by Dong et al. (1994), given the short blade lengths and the moderate Reynolds number, the boundary layers developing on their surfaces are not fully developed, and, in addition, RANS models, even when implemented in the unsteady form are unlikely to capture all the time scales, ranging from that of the vortex shedding at the blade tips to the large-scale meridional circulation induced in the tank.

A more sophisticated approach for turbulent simulations was taken by Eggels (1996), where a lattice-Boltzmann scheme was used to study the flow in a stirred tank with baffles. Time accurate simulations were carried out on a uniform mesh of minimum dimension being the impeller blade thickness. The motion of the impeller was simulated by a body force specified from the impeller geometry and motion. Accurate results were reported in terms of mean velocity components and turbulent fluctuations, proving the potential of this technique; the drawback of this method was the extremely high demand of computational power attributed to the uniform mesh required by the lattice-Boltzmann procedure.

In a recent article by Verzicco et al. (2000), it has been shown that the combination of the "immersed-boundary" (IB) procedure with direct numerical simulations (DNS) or large-eddy simulations (LES) can efficiently be used for the accurate prediction and analysis of many technologically relevant flows. In particular, because the presence of complex boundaries is mimicked by body forces, the simulations are in fact carried out on "simple grids," thus taking advantage of the efficiency and accuracy of optimized solution procedures. IB/DNS simulations of complex-geometry turbulent flows can be carried out with 1–2 million gridpoints on a PC with CPU times ranging from a few hours to a few days. In this article we will show some examples of these simulations for an impeller-stirred cylindrical tank and the results will be compared with experiments and RANS simulations; in addition to a discussion aimed at showing the efficiency of the immersed-boundary method, an explanation will be given for the poor prediction of RANS closures of this simple-geometry low–Reynolds number flow.

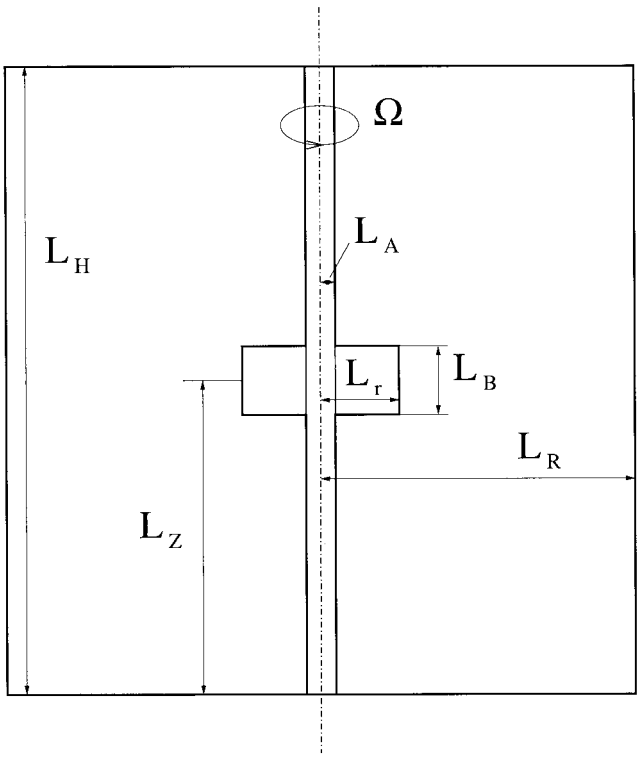

Figure 1. Mixer geometry: $L_r = 1$, $L_B = 0.8$, $L_A = 0.32$, $L_R = 4$, $L_Z = 4$, and $L_H = 8$.

Physical Problem and Numerical Setup

The flow investigated in this study consists of a cylindrical, unbaffled tank stirred by an impeller located at midheight of the tank, rotating at constant angular velocity Ω; the simulations intend to reproduce the classical experiments by Dong et al. (1994). The impeller has eight blades equispaced over the whole azimuthal span. A sketch of the device is given in Figure 1, where all the lengths have been scaled with the blade radius $R = 1.25$ cm. The impeller rotation speed is $\omega = 100$ rpm and the working fluid is water ($\nu = 10^{-6}$ m^2/s), thus yielding a Reynolds number $\mathrm{Re} = \Omega R^2/\nu = 1636$, with $\Omega = 2\pi\omega/60$ the rotation speed, expressed in rad/s.

For the numerical solution of the flow, the Navier–Stokes equations are solved in a frame of reference fixed with the impeller and therefore rotating with constant angular velocity Ω. The equations in the rotating frame, scaled with the velocity $U = \Omega R$ and the length $L = R$, are

$$\frac{D\mathbf{u}}{Dt} = -\nabla p - \frac{1}{Ro}\hat{\Omega} \times \mathbf{u} + \frac{1}{\mathrm{Re}}\nabla^2\mathbf{u} + \mathbf{f} \qquad (1a)$$

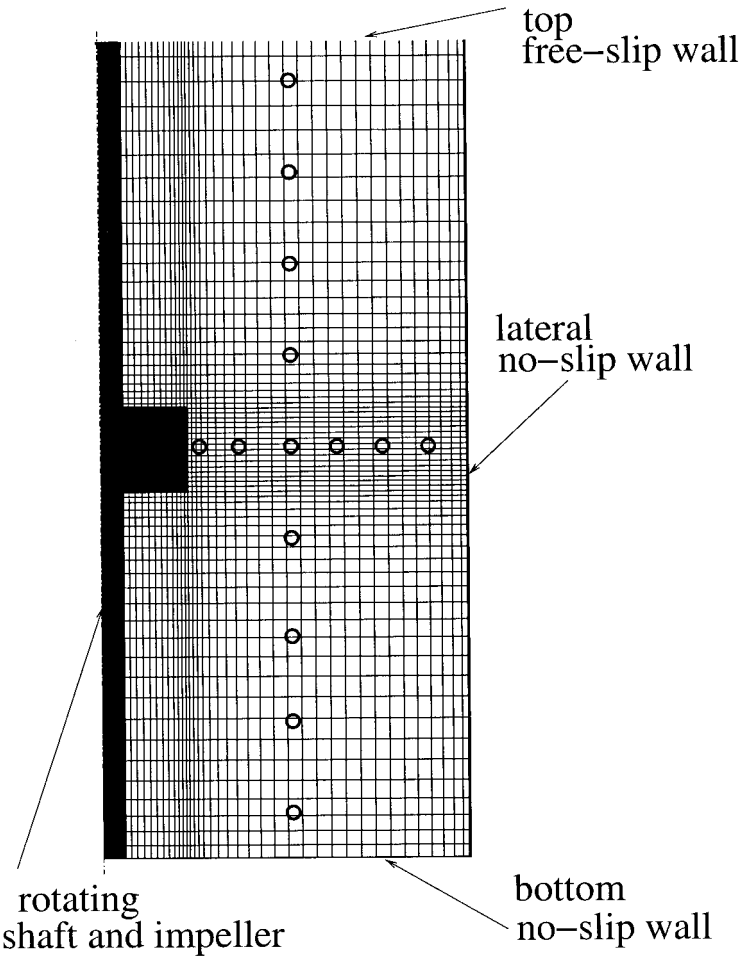

Figure 2. Example of grid in a meridional plane and boundary conditions (only one of every 6 gridpoints is shown).
Open circles indicate the position of numerical probes used for the flow analysis.

$$\nabla \cdot \mathbf{u} = 0 \tag{1b}$$

where $Ro = 1/2$, $\hat{\Omega}$ is the unit vector directed as the impeller rotation vector, and **f** is a body force (to be described later). In this frame of reference the external cylindrical wall of the tank has an azimuthal velocity $V_\theta(L_R) = -\Omega L_R$, whereas the bottom horizontal no-slip surface moves according to $V_\theta(r) = -\Omega r$, with r the radial coordinate.

The computational domain is discretized by a mesh that is nonuniform in the radial and axial directions to cluster the gridpoints in the blade region and close to the no-slip surfaces (Figure 2). The mesh is uniform in the azimuthal direction. The resolution in the azimuthal direction was fixed by requiring that at least three gridpoints (one on each surface and one in the middle) were located within the blade thickness $L_{th} = 0.1L_r$. In this case the azimuthal grid spacing at the blade tip was $\Delta x_\theta = L_r\Delta\theta \simeq 0.05L_r$, thus ensuring a minimum of three nodes inside the boundary layer (estimated by $\delta/L_r = 5/\sqrt{\mathrm{Re}}$). Nevertheless, because these are only order-of-magnitude estimates, additional simulations were run on 1/8th of the domain (containing only one impeller blade) with a resolution ranging from 16 to 128 azimuthal nodes. These resolution yielded, respectively, from 3 to 16 cells inside the blade thickness, producing a flow dynamics with negligible differences. Similar refinement checks were performed for the radial and axial directions: grids ranging from $49 \times 57 \times 97$ to $97 \times 102 \times 192$ (in the azimuthal, radial, and axial directions, respectively) were used to assess the quality of the presented results.

An important aspect of this study was the initialization of the simulation. In the experiments, it has been observed that starting from rest, the flow needs from 5 to 10 min, corresponding to 500 to 1000 impeller revolutions, to attain a statistically stationary configuration (that is, a flow where long-term averages are not time dependent). In the present DNS simulation each revolution is discretized by about 300 time steps, thus requiring 3×10^5 time steps for the initial transient to be exhausted. This computational overhead is clearly unacceptable because it would require, on the finest grid, more CPU hours than the useful part of the simulation. Several strategies have been followed to reduce the computation of the transient. The most straightforward approach consisted of successive simulations starting from a very coarse grid with a progressive refinement by interpolations. The initial flow evolution was obtained by simulating only 1/8th of azimuthal domain and therefore only one impeller blade; the field was then replicated in such a way as to reproduce the whole impeller. Unfortu-

nately, the adjustments of the solutions from one grid to another introduced additional transients that also turned out to be time consuming. As an alternative we also tried to start from a low-Reynolds coarse-grid flow and to increase grid and Reynolds number together. However, in this case the flow adjustment was very slow as well, and a total of almost 500 impeller revolutions was necessary to attain a developed flow field. Most of the transient, however, was simulated over coarse grids; therefore the total CPU time was equivalent to 40 impeller revolutions on the finest grid.

In terms of CPU time, each impeller revolution required 6780 CPU seconds (about 1.9 h) on a $97 \times 102 \times 192$ grid and a 1.4-GHz AMD-Athlon processor, implying about 70 CPU hours for the transient calculation and 9.51×10^{-6} s per time step and per node.

The boundary body force $\mathbf{f}$ of Eq. 1 is prescribed at each time step to establish the desired velocity $\mathbf{V}_b$ on an arbitrary surface. The time-discretized version of Eq. 1a can be written as

$$\mathbf{u}^{n+1} - \mathbf{u}^n = \Delta t(RHS + \mathbf{f}) \tag{2}$$

where Δt is the computational time step; *RHS* contains the nonlinear, pressure, and viscous terms; and the superscript denotes the time-step level. To impose $\mathbf{u}^{n+1} = \mathbf{V}_b$, the body force $\mathbf{f}$ must be

$$\mathbf{f} = -RHS + \frac{\mathbf{V}_b - \mathbf{u}^n}{\Delta t} \tag{3}$$

in the flow region where we seek to mimic the solid body and zero elsewhere. In general, the surface of the region where $\mathbf{u}^{n+1} = \mathbf{V}_b$ does not coincide with a coordinate line. In that case, the value of $\mathbf{f}$ at the node closest to the surface, but outside the solid body, is linearly interpolated between the value that yields $\mathbf{V}_b$ inside the solid body and the value in the interior of the flow domain. This interpolation procedure is consistent with the centered second-order finite-difference approximation, and the overall accuracy of the scheme remains second-order (Fadlun et al., 2000).

Equations 1a and 1b were spatially discretized in a cylindrical coordinate system using staggered central second-order finite-difference approximations. Details of the numerical method are given in Verzicco and Orlandi (1996); only the main features are summarized here.

The discretized system is integrated in time using a fractional-step method, where the viscous terms are computed implicitly and the convective terms explicitly. The large sparse matrix resulting from the implicit treatment is inverted by an approximate factorization technique. At each time step, the momentum equations are provisionally advanced using the pressure at the previous time step, giving an intermediate nonsolenoidal velocity field. A scalar quantity Φ is then introduced to project the nonsolenoidal field onto a solenoidal one. The large-band matrix associated with the elliptic equation for Φ is reduced to a pentadiagonal matrix using trigonometric expansions (FFTs) in the azimuthal direction; this matrix is inverted using the FISHPACK package (Swartzrauber, 1974). A hybrid low-storage third-order Runge–Kutta scheme is used to advance the equations in time, and the body forces are enforced at each stage of the Runge–Kutta scheme. The integration of the equations with the body forces takes only 5% more CPU time than that in the absence of forcing.

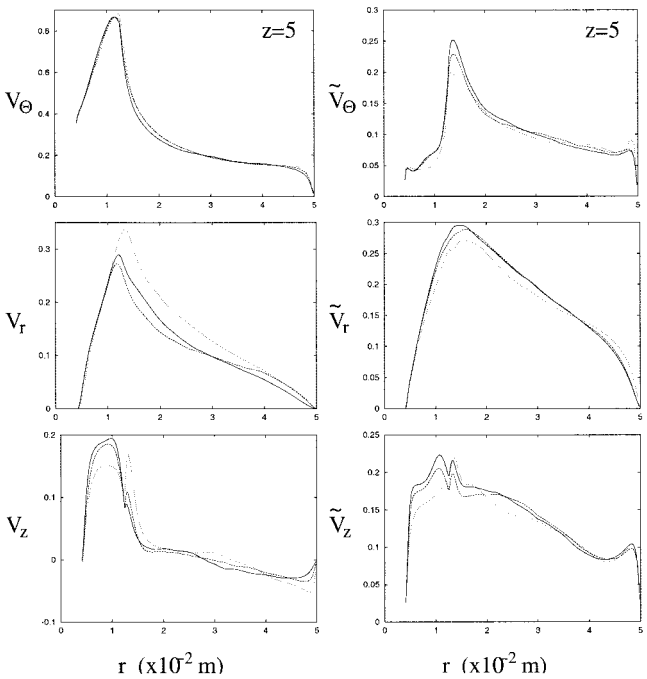

Figure 3. Radial profiles of averaged (left) and rms (right) azimuthal radial and vertical velocity at mid-height in the tank.

—, DNS on $97 \times 92 \times 192$ grid; - - -, LES simulation on $97 \times 92 \times 192$ grid; $\cdots$, DNS on $65 \times 57 \times 97$ grid.

The simulation of the flow inside mixing devices is usually performed using RANS models because of their reduced computational cost. Because one aim of the present article is to compare the performance of DNS/LES vs. RANS models, we have also performed RANS simulations of the flow previously described. Steady RANS equations in a frame rotating with the impeller are solved on a 1/8th sector of the tank using a commercial CFD code and body-fitted grids. Periodicity conditions are imposed in the azimuthal direction. A low–Reynolds number turbulence model has been used, that is, the v^2–f model by Durbin (1995). In the v^2–f model, the equations are integrated up to the wall without the aid of algebraic functions, thus providing a wide applicability. We stress that the present RANS simulations are reported only to provide the reader with a reference performance of RANS simulations. A detailed comparison of the various models can be found in Jones et al. (2001).

Results

Several preliminary simulations were performed to investigate the mesh distribution and grid resolution, the necessity for a turbulence model, possible effects of the upper free-surface deformation, and how many blades of the impeller had to be simulated. Concerning the first point, grids ranging from 5×10^5 to 1.9×10^6 cells have been used to assess the reliability and grid independence of the results. In particular, two simulations with grids $65 \times 57 \times 97$ and $97 \times 102 \times 192$, in the azimuthal, radial, and axial directions, respectively, have been

run for 20 impeller revolutions showing mean velocity fields, which agreed within a few percent for the mean and root mean square (rms) velocity profiles (Figure 3).

The need for turbulence modeling has been verified by running an identical case with and without the subgrid-scale (SGS) model. Given the operational conditions of the test, the Reynolds number is quite small (Re = 1636) and direct numerical simulation is possible. Consistently, a LES simulation with the dynamic SGS (Reed et al., 1974) model gave results almost coincident with those of the direct numerical simulation (Figure 3), the dynamic SGS model yielding a turbulent viscosity close to zero. We emphasize that this is one of the main advantages of the dynamic Smagorinsky model, which automatically switches off when the grid resolution is adequate. It was previously shown (Mittal and Moin, 1997) that LES models can be used only in combination with nondissipative discretization schemes; accordingly, central second-order finite-difference approximations have been used that do not introduce any numerical viscosity. The only noticeable improvement given by the SGS model is in the balance between the energy supplied to the system by the impeller and that dissipated by the flow attributed to viscosity. In fact, if the flow is statistically steady, the two quantities must be equal and this was obtained only in the LES simulation. In more detail, the power number of the impeller (nondimensional power introduced by the impeller in the flow) was $P_{LES} = 0.359$ and $P_{DNS} = 0.351$, respectively, for the LES and DNS simulation on the fine grid, whereas the integrated dissipation (nondimensional power dissipated by the flow) was $D_{LES} = 0.355$ and $D_{DNS} = 0.419$. The same quantities computed for the DNS on the coarse grid yielded a mismatch of the order of 35%.

It must be noted that direct numerical simulation is possible only for the present "simplified" model problem in which geometrical dimensions and rotation speed are both small. For the simulation of practical cases, operational conditions are more severe and the use of a SGS model would be mandatory.

Free-surface deformation is induced by the azimuthal rotation and the resulting balance of hydrostatic and centrifugal forces at the interface between fluid and air. This deformation is often disregarded in numerical simulations and the upper boundary of the tank is modeled by a flat free-slip wall. This strategy was also followed in the main case presented in this article. However, some remarks on the free-surface effects are in order. Assuming that the bulk of the flow is in solid-body rotation, the shape of the free surface would be given by $z = \Omega^2 r^2/(2g)$, which for the present flow conditions yields a maximum deformation $\Delta z \simeq 1.4$ cm. This displacement is larger than the blade radius; therefore, in principle, it is possible that the results would be changed by this additional effect. In one case, the free-surface deformation was modeled by the body forces as the rotating impeller (and therefore rotating with the same angular velocity), with the results being only slightly modified by this new effect and only in the region close to the upper surface. We will see that in fact the flow rotates significantly more slowly than a solid-body rotation. The free-surface deformation would be smaller than previously estimated and the approximation of the upper surface as a flat, stress-free boundary is indeed appropriate.

Because the impeller consists of eight equispaced blades it is tempting, for computational purposes, to reduce the domain to 1/8th of the tank and only one blade. This assumption yields a considerable reduction of computational effort. Nevertheless on a domain reduced to 1/8th of the azimuthal span, only structures with eightfold symmetry and multiples can be supported. This prevents the development of azimuthal modes with a wave number < 8 and of all the modes that are not multiples of 8. We have verified with simulations that included one or two impeller blades (and therefore on 1/8th and 1/4th of the domain, respectively) that this assumption is not appropriate for the present problem and the results were significantly different from experimental results. The inadequacy of the simulation on 1/8th of the domain is also confirmed by Figure 4, showing the time evolution of the azimuthal energy modes for a simulation over the whole domain but initiated from a simulation performed over a 1/8th sector. We can see that the energy in the $n = 8$ mode slowly decreases in time, whereas the lower modes experience an exponential growth and, after saturation, attain an energy either comparable to or bigger than the original $n = 8$ mode. In particular, because the azimuthal $n = 1$ mode attained the biggest value, the mean flow is not axisymmetric and contains off-center structures that possibly have a precessional velocity. Figure 4 clearly shows that the eightfold symmetry was only an artifact of the computational domain. The system would also tend to distribute the energy among odd and low-order modes. This point is further stressed by analyzing the velocity profiles shown in Figure 5; it is shown that the radial velocity is severely overpredicted in the simulation over 1/8th of the domain. This overprediction is less evident when the simulation is extended over two impeller blades, whereas the best results are obtained for the whole domain. It is worth mentioning that the prediction of the azimuthal velocity profiles is as accurate as in Figure 5 for all the radial sections and it is independent of whether a section or the whole domain is simulated. Radial and axial velocity profiles, in contrast, are much more sensitive to the azimuthal extension of the domain and this point will be further discussed when comparing the DNS with RANS results. From the above results it is concluded that, to obtain accurate simulations, it is

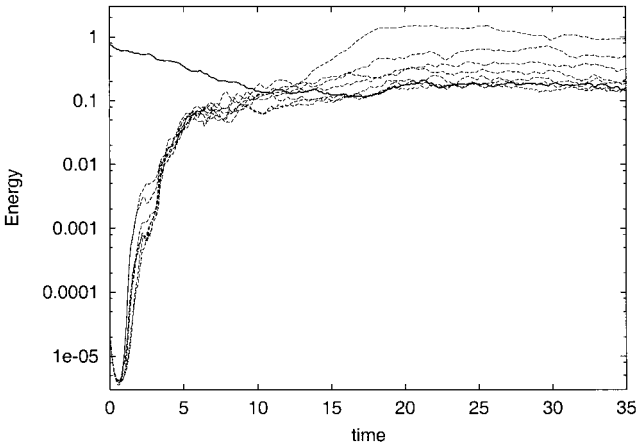

Figure 4. Time evolution of the kinetic energy of azimuthal modes starting from a simulation on 1/8th of the domain and one impeller blade: n = 8 mode, all modes from $n = 1$ to $n = 7$.

Note that time has been rescaled so that each time unit corresponds to one rotation period of the impeller. The mode with the highest energy content is $n = 1$.

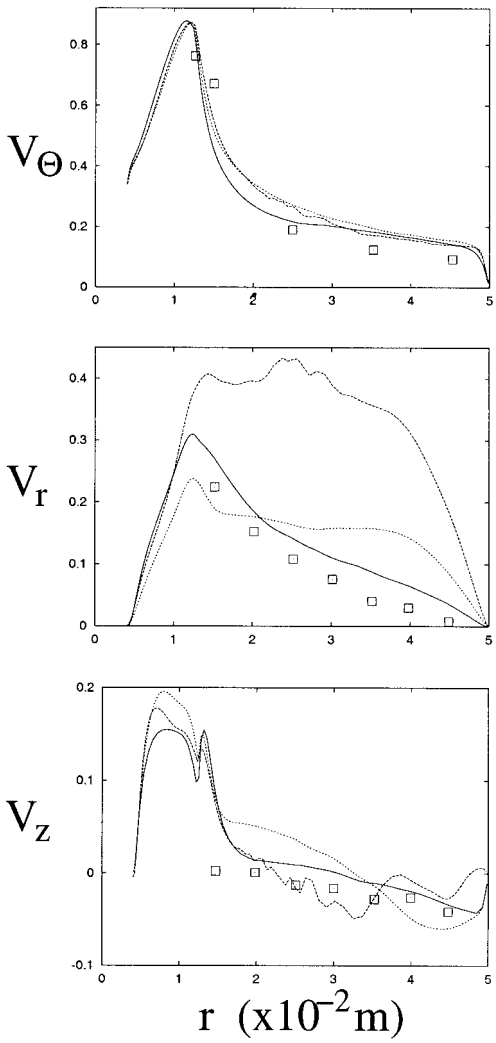

Figure 5. Averaged radial velocity profiles in a section crossing the impeller ($x = 4$).

Top: azimuthal velocity; center: radial velocity; bottom: axial velocity: simulation on 1/8th of the domain (1 blade), 1/4th of the domain (2 blades), whole domain, symbols represent experimental data of Dong et al. (1994).

not possible to reduce the domain using impeller symmetries but the whole geometry must be solved.

The last point to be addressed is the question of how many impeller rotations must be simulated to obtain converged statistics. The present procedure consisted in computing the flow statistics for two time intervals, $T_1 = T$ and $T_2 = 2T$; when the mean value of each velocity component computed over T_1 was contained within the analogous mean plus and minus the rms value computed over T_2 the simulation could be stopped. Our results show that approximately 20 impeller revolutions were sufficient to obtain converged mean quantities but an interval at least twice longer had to be used for the energy spectra and second-order moments. The simulation presented in the following section has been run for 150 impeller revolutions to ensure that averages and spectra were converged.

Comparison with RANS simulation and experiments

We will now describe the results of the DNS simulation and compare them with the available experimental and RANS data. In Figure 6 we report the computed mean field, averaged in both azimuthal direction and in time.

It is evident that the meridional plane is roughly divided into two halves by the radial jet emanating from the impeller. The two recirculations are not symmetric because of the different boundary conditions on the upper and lower horizontal surfaces. An important effect of the lower no-slip wall is the strongly positive vertical velocity in the lower half of the domain in the region close to the shaft (Figure 6d). This effect is characteristic of wall-bounded rotating flows and is known as "Eckman pumping," which causes the fluid to be pushed radially inward at the plate (Figure 6c) and axially upward at the axis of rotation (Figure 6d). Because of mass conservation, a vertical ascending fluid column at the axis induces a descending current at the external radial wall, thus reinforcing the lower-half recirculation with respect to the upper one. This is

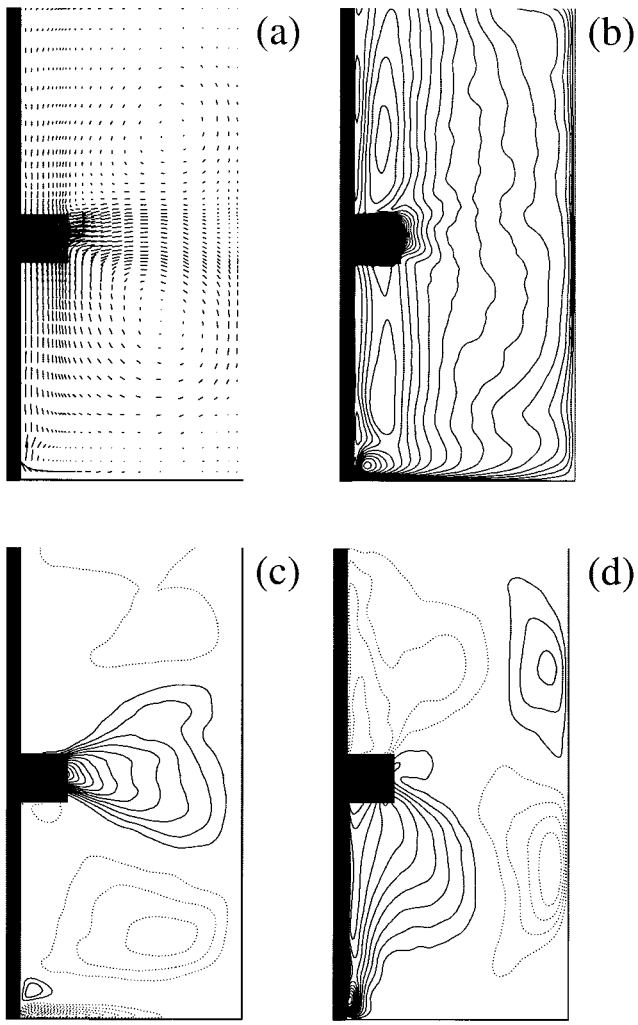

Figure 6. Averaged velocity fields: (a) velocity vector field, contours of: (b) azimuthal, (c) radial, (d) axial velocity components ($\Delta u = \pm 0.025$).

—, for positive; · · ·, for negative values.

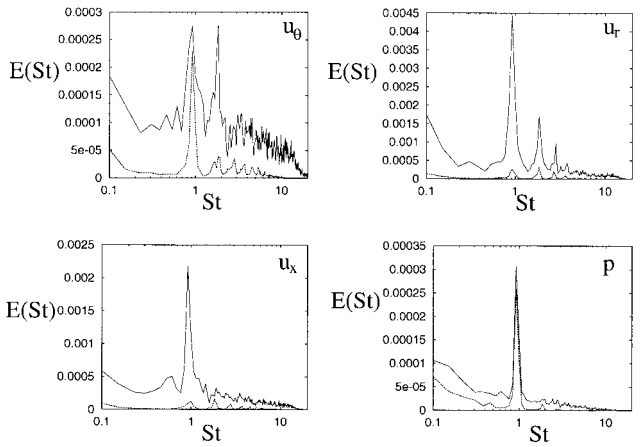

Figure 7. Frequency spectra of velocity components and pressure for the probes at ($r = 2, x = 4$) (—) and ($r = 2, x = 2$) (– · –).

The probes are in the radial jet emanating from the impeller and in the center of the lower meridional recirculation, respectively. Note that the frequencies in the abscissa have been rescaled so that $St = 1$ corresponds to the rotation period of the impeller.

also well evidenced by the radial jet that does not point exactly in the radial direction but, rather, has a positive vertical velocity close to the blade region and then a weakly negative vertical velocity.

Instantaneous snapshots analogous to those of Figure 6 (not reported here for the sake of brevity) show the strongly unsteady nature of the flow, as can be deducted by the analysis of the velocity signals taken from the numerical probes whose positions are reported in Figure 2. Spectra are computed from the temporal series and are plotted in semi-log axes to separate the frequency peaks attributed to coherent motion from the background turbulence. In particular, in Figure 7 we show the spectra of two probes, respectively, in the jet of the impeller ($r = 2L_r$, $x = 4L_r$) and in the core of the lower recirculation ($r = 2L_r$, $x = 2L_r$). Although the flow in the meridional recirculation is essentially dominated by the rotation period of the impeller, the flow in the jet has a wide frequency content, ranging from the slow vertical jet flapping to the fast vortex shedding at the blade tips. Given the different time scales of the described flow phenomena, it is very difficult for RANS models to correctly parameterize all the flow fluctuations and this is confirmed by the velocity profile results. The spectra of Figure 7 also indicate that the flow is strongly inhomogeneous in space with slow and laminar recirculations far from the impeller and a turbulent-like jet region at the center of the tank. It is also useful to point out that these spectra confirm the results reported before in Figure 4: in none of the spectra is a peak observed at $St = 8$ that represents the frequency associated with the passage of a single blade, (Using $U = \Omega L_r$ and L_r, respectively, as scaling velocity and length, the unity time unit results $T = L_r/U = 1/\Omega$, implying a time $t = 2\pi T$ for one impeller revolution. In this article we have defined the nondimensional frequency $St = 2\pi/t$ so that $St = 1$ corresponds to the rotation frequency) which indicates, once again, that the flow field does not have a eightfold symmetry.

This scenario is fully confirmed by the contours of turbulent kinetic energy for a meridional plane containing one lateral surface of the blade. This shows the transitional nature of the flow on the blade, which is laminar in the region closer to the shaft and transitional toward the blade tip; this transition cannot be captured by RANS models unless these are properly parameterized by ad hoc assumptions.

Radial profiles of azimuthal, radial, and vertical mean and rms velocity components are compared with experimental and RANS data simulations in Figures 9, 10, and 11. The DNS prediction for the azimuthal velocity component is quite accurate, particularly in the region near the shaft above and below the impeller, where a peak is observed. This is attributed to the large-scale recirculation that drives the fluid from the external radial region toward the axis, increasing the azimuthal velocity to conserve the angular momentum. Except for the section crossing the impeller, RANS simulations severely underpredict the peak velocity, confirming the findings of Jones et al. (2001). As already mentioned, the accurate DNS prediction of the azimuthal velocity profiles is independent of the computational domain extension; therefore, the RANS velocity underprediction must be attributed to the inadequacy of the modeling for this flow and not to the restriction of the computational domain to 1/8th of the full size.

Radial and vertical velocity components are also accurately predicted by the DNS simulation with results that are generally better than those using RANS. This is especially true for the radial velocity profile in the section crossing the blade, where RANS results overpredicted the velocity by more than a factor of 2. This mismatch, however, can only partially be attributed to RANS modeling because a major effect is induced by the limitation of the computational domain to only one blade, as shown in Figure 5.

It is important to mention that, because of the low value of the Reynolds number (Re = 1636), the flow cannot be considered fully turbulent and a comparison of DNS with conventional RANS two-equation turbulence models could not be completely reliable. On the other hand, low–Reynolds number versions of κ–ε RANS models have been developed for these flows and some results are also reported in Figures 8–11. These

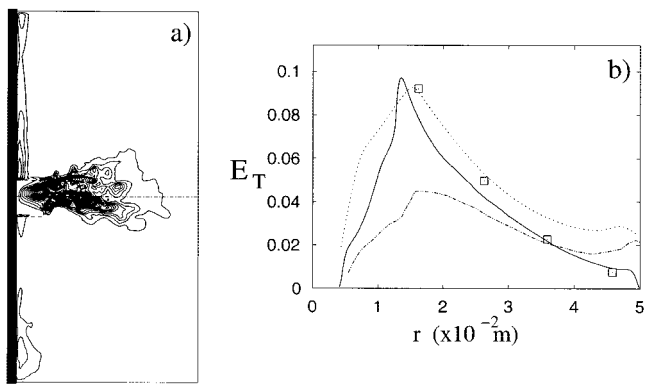

Figure 8. (a) Contour plots of turbulent kinetic energy in a meridional plane containing one lateral surface of the blade ($\Delta k = 5 \times 10^{-4}$). (b) Radial profile of averaged turbulent kinetic energy at midheight of the tank.

—, present DNS results, – · · –, RANS simulation with the v^2–f model, · · ·, low-Re κ–ε [data from Jones et al. (2001)]; symbols represent experimental data of Dong et al. (1994).

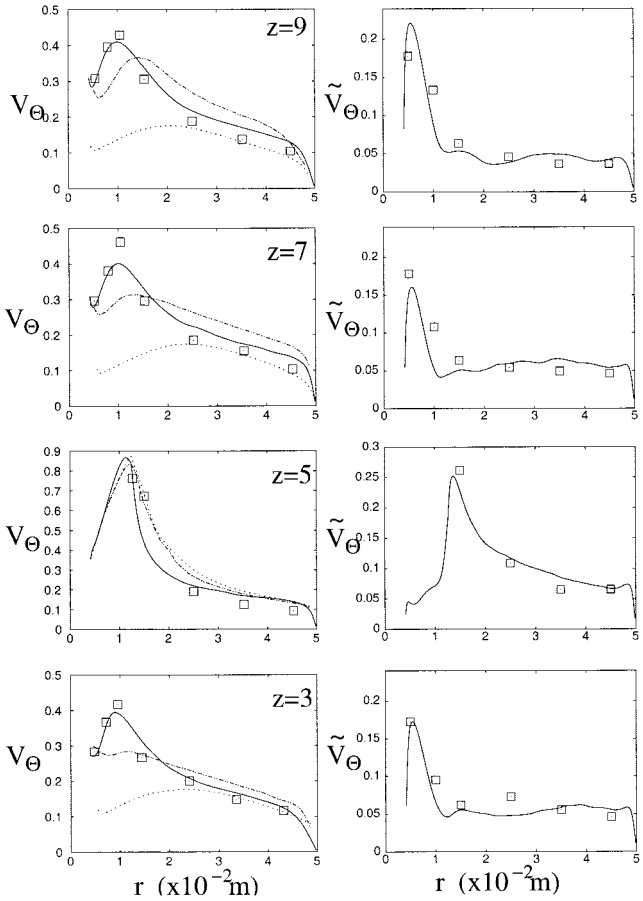

Figure 9. Radial profiles of averaged (left) and rms (right) azimuthal velocity at different heights in the tank.

—, present DNS results; –··–, RANS simulation with the v^2–f model; ···, low-Re κ–ε [data from Jones et al. (2001)]; symbols represent the experimental data of Dong et al. (1994). The azimuthal velocity is scaled by the blade tip velocity. (The values of z are in tenths of the tank height.)

data were taken from Jones et al. (2001), who reported extensive testing of low–Reynolds number and conventional RANS two-equation turbulence models, consistently obtaining an agreement with experiments as in Figures 8–11.

The comparison of the present rms velocity profiles with the experiments is also very satisfactory for both peak values and radial distributions, which are well captured by the numerical simulation. This comparison cannot be performed for the RANS modeling because it computes only the turbulent kinetic energy and not the single velocity fluctuations. Nevertheless, once the energy is computed from the velocity fluctuations the former can be compared with the RANS and the experimental values, as shown for one section in Figure 8b.

It is worth noting (although it is evident from the rms velocity profiles) that appreciable turbulent energy values are present only in the section crossing the impeller halfway between the horizontal boundaries. In the other sections, in contrast, the energy is one order of magnitude smaller and it is essentially zero far from the rotating shaft. This confirms once more the inhomogeneous character of the present flow field with turbulent regions surrounded by laminar ones.

An additional comparison with the experiments has been performed by computing the pumping coefficient N_{Q_P}, defined as the ratio of the radial flow rate through a specific section S and twice the tip blade velocity multiplied by the squared impeller diameter. In this case, following Dong et al. (1994), the surface S was chosen as the circular strip vertically centered at the impeller, of the same height as the blade and at a distance $1.4L_r$ from the axis. In the experiment by Dong et al. (1994) it was found that $N_{Q_P} = 0.62$, whereas the present simulation yields $N_{Q_P} = 0.641$; on the other hand, Reed et al. (1974) reviewed the existing results and reported the range $N_{Q_P} = 0.75 \pm 0.15$.

Before concluding this section, we will briefly comment on the comparison between the results of steady RANS over 1/8th of the domain and the DNS over the whole mixer. There would be, in fact, two ways to make the RANS simulations closer to the DNS counterpart: the first is to simulate the entire domain and the second to consider unsteady RANS. The first change would be ineffective because the flow is not instantaneously symmetric but it is statistically symmetric. This implies that a steady flow, computed over the eight blades of the impeller, would give an eightfold symmetric field.

Time-accurate RANS simulations, on the other hand, aim to capture flows with definite and limited frequency content (that is, corresponding to vortex shedding or large-scale coherent motions) and to model the random (broad-band) turbulent

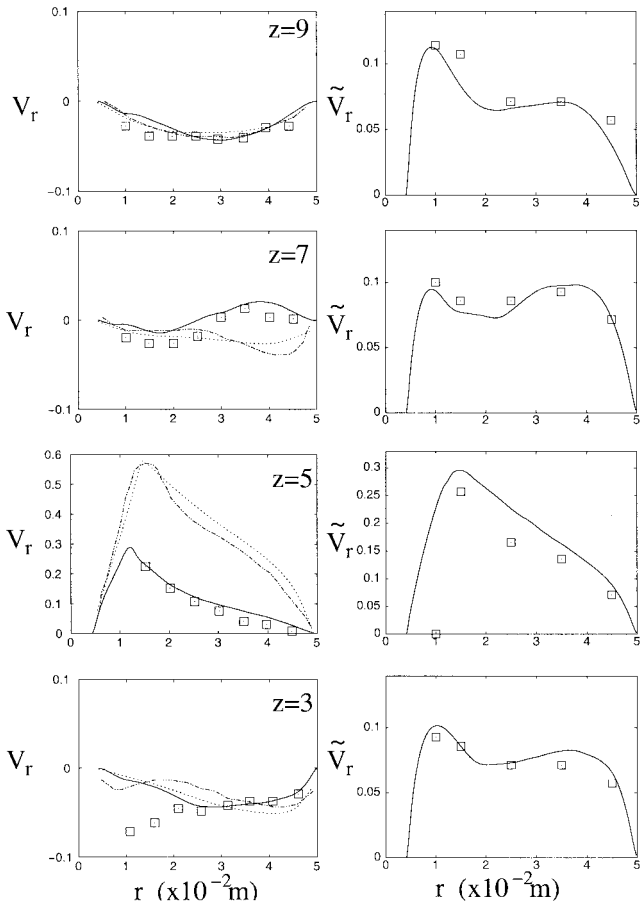

Figure 10. The same as Figure 9 for averaged radial velocity.

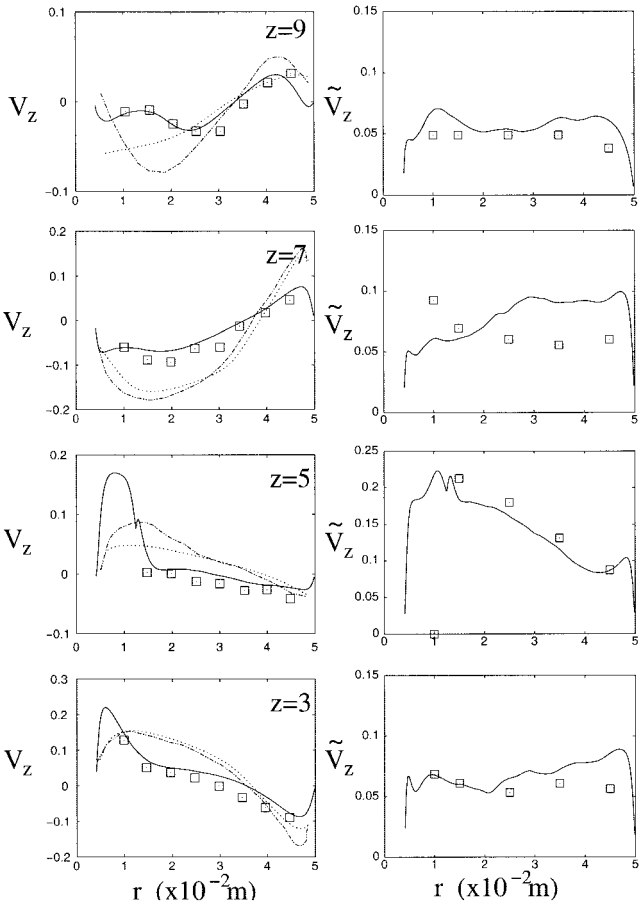

Figure 11. The same as 9 for averaged axial velocity.

motion using standard turbulence closures. In the present situation the flow unsteadiness is not well organized, especially in relation to the radial jet emanating from the impeller, and therefore it is not expected that unsteady RANS would provide improved results. In addition, the computational cost of unsteady RANS is of the same order of the present DNS/LES technique.

We emphasize that the main aim of this study was not to show the superiority of DNS with respect to RANS because it is an obvious and well-known result coming directly from the enormous computational cost and the very limited applicability of the direct numerical simulations of the Navier–Stokes equations. Our purpose was rather to show that simple geometrical configurations and moderate Reynolds numbers are not benign conditions for the use of RANS modeling. The reasons are that low-Re problems allow the coexistence of laminar, transitional, and turbulent flow regions, whereas RANS closures are tailored only for the latter regime. The geometrical simplicity of the present mixer causes the turbulent regions to be localized only around the impeller, causing strong flow inhomogeneity. The situation would be different in the presence of baffles, which would act as additional turbulence sources, thus producing more homogeneous conditions.

The above considerations are consistent with the results in the literature, showing accurate RANS predictions for complex-geometry high-Reynolds flows in mixers and poor performance for the present problem (Jones et al., 2001).

Conclusions

In this article we have performed a DNS of the flow in an impeller-stirred unbaffled cylindrical tank with an immersed-boundary procedure to deal with the complex geometry. The main motivation comes from the literature, which shows that, although the geometry is relatively simple, standard RANS simulations yield a very poor flow prediction. Because the present flow configuration has recently been used to assess the performance of RANS closures (Jones et al., 2001), and none of them gave satisfactory results, we decided to investigate the flow physics to understand the causes of the systematic mismatch between experimental results and RANS simulations.

It is found that the flow is strongly unsteady and inhomogeneous even if the Reynolds number is low enough to make DNS affordable. Accordingly, a LES simulation with a dynamic subgrid-scale model yielded the same results as the DNS. RANS models, in contrast, cannot automatically switch off when the resolution is fine enough and they parameterize all the velocity oscillations as turbulent fluctuations. Because the impeller has eight azimuthally equispaced blades, simulations have always been performed, in the literature, over a sector of the domain spanning 1/8th of the domain. Although this assumption reduces the computational cost by a factor 8, the results do not agree with the experiments, given that the flow is forced to maintain an unphysical symmetry. A posteriori this result is not surprising because, looking at Figure 1, it is unlikely that blades whose area is less than 1/50th of the meridional section could enforce any symmetry on the large-scale flow.

Some remarks on the computational costs of these DNS simulations are in order. In contrast to RANS, where a steady solution is forced, for unsteady simulations mean quantities are obtained by averaging the solution in time. In the present case, the intense velocity fluctuations required long-term averages (typically at least 20 impeller revolutions) to obtain smooth converged statistics. This must be added to the initial transient that consisted of an equivalent time of about 40 impeller revolutions on the finest grid. The computation of this flow evolution by standard methods would be highly expensive compared to RANS simulations, where the mean field is directly obtained. Fortunately, the use of the immersed-boundary procedure makes the simulation of complex-geometry three-dimensional unsteady flows quite affordable. As an example, in the present case on a grid of 1.9×10^6 points the code uses 85 Mb of RAM and requires 18 s for each time step on a single 1.4-GHz Athlon processor; the entire simulation (including the initialization) required slightly less than 5 days.

The application of the immersed-boundary method to chemical engineering problems would be even more advantageous for more complex configurations. In fact, if the tank also had baffles, the relative motion between the baffles and the impeller required, for standard methods, a sliding mesh approach, mesh deforming, or regridding. In contrast, the present technique, by a time-dependent tagging of the forced cells, would allow the simulation on moving geometries essentially at the same computational cost as that of fixed configurations.

Literature Cited

Dong, L., S. T. Johansen, and T. A. Engh, "Flow Induced by an Impeller in an Unbaffled Tank—I. Experimental," *Chem. Eng. Sci.*, **49**(4), 549 (1994).

Durbin, P. A., "Separated Flow Computations with the κ–ε–v^2 Model," *AIAA J.*, **33**, 659 (1995).

Eggels, J. C. M. "Direct and Large-Eddy Simulation of Turbulent Fluid Flow Using the Lattice-Boltzmann Scheme," *Int. J. Heat Fluid Flow*, **17**, 307 (1996).

Fadlun, E. A., R. Verzicco, P. Orlandi, and J. Mohd-Yusof, "Combined Immersed-Boundary/Finite-Difference Methods for Three-dimensional Complex Flow Simulations," *J. Comp. Phys.*, **161**, 35 (2000).

Harvey, A. D., III, and S. E. Rogers, "Steady-State Modeling and Experimental Measurements of a Baffled Impeller Stirred Tank," *AIChE J.*, **41**(10), 2177 (1995).

Harvey, A. D., III, and S. E. Rogers, "Steady and Unsteady Computation of Impeller-Stirred Reactors," *AIChE J.*, **42**(10), 2701 (1996).

Jones, R. M., A. D. Harvey III, and S. Acharya, "Two-Equation Turbulence Modeling for Impeller Stirred Tanks," *J. Fluids Eng.*, **123**(3), 640 (2001).

Launder, B. E., and A. Sharma, "Application of the Energy-Dissipation Model of Turbulence to the Calculation of Flow Near a Spinning Disk," *Lett. Heat Mass Transfer*, **1**, 131 (1974).

Mittal, R., and P. Moin, "Suitability of Upwind-Biased Finite-Difference Schemes for Large-Eddy Simulation of Turbulent Flows," *AIAA J.*, **35**, 1415 (1997).

Reed, X. B., M. Princz, and S. Hartland, "Laser Doppler Measurements of Turbulence in a Standard Stirred Tank," *Proc. 2nd Eur. Conf. on Mixing*, Cambridge, UK (BHRA-Canfield), 7 (1974).

Swartzrauber, P. N., "Direct Method for the Discrete Solution of Separable Elliptic Equations," *SIAM J. Numer. Anal.*, **11**, 1136 (1974).

Verzicco, R., J. Mohd-Yusof, P. Orlandi, and D. Haworth, "Large-Eddy Simulation in Complex Geometric Configurations Using Boundary Body Forces," *AIAA J.*, **38**(3), 427 (2000).

Verzicco, R., and P. Orlandi, "A Finite-Difference Scheme for Three-dimensional Incompressible Flows in Cylindrical Coordinates," *J. Comp. Phys.*, **123**, 402 (1996).

Wechsler, K., M. Breuer, and F. Durst, "Steady and Unsteady Computations of Turbulent Flows Induced by a 4/45° Pitched-Blade Impeller," *J. Fluids Eng.*, **121**, 318 (1999).

Xu, Y., and G. McGrath, "CFD Predictions of Stirred Tank Flows," *Trans. IChemE.*, **74**(A), 471 (1996).

Manuscript received Sep. 26, 2002, and revision received July 23, 2003.